Evolution of superfluid turbulence in thermal counterflow

K. P. Martin* and J. T. Tough
Department of Physics, The Ohio State University, Columbus, Ohio 43210
(Received 12 October 1982)

Using two complementary techniques, we have for the first time determined the full evolution of superfluid turbulence in a single circular tube. Our analysis shows that the evolution of the turbulence from laminar flow through the two turbulent states T I and T II is independent of the tube size and is probably a generic feature of the circular geometry. This important result finally allows a reliable comparison to be made of data from wide and narrow tube experiments. The parameters of states T I and T II are found to be well defined by these experiments, and comparison to the theory of Schwarz suggests that the fully developed state T II is reasonably homogeneous. The transition from laminar flow to state T I is consistent with previous results showing a critical density of quantized vortex lines in the turbulence. Our analysis suggests that this concept may be extended to the transition from T I to T II. Associated with this second transition is an intrinsic relaxation time that appears to diverge at the critical velocity.

INTRODUCTION

A major obstruction to the systematic understanding of superfluid turbulence in thermal counterflow has been the inability to make a reliable comparison of results obtained from wide and narrow flow tubes. Because of their size, narrow-tube experiments are generally limited to measurements of the temperature, pressure, or chemical potential difference along the tube. Circular tubes with diameters d of the order of 10^{-2} cm exhibit a progression of two different turbulent states T I and T II, in addition to a laminar nonturbulent state at low flow velocities. While the transition from laminar flow to T I and the transition from T I to T II is clearly evident in these tubes, the temperature differences become too large for meaningful measurements to be made of state T II. On the contrary, the temperature difference in wide tubes only becomes appreciable at high velocities and the single turbulent state determined in a variety of different measurements is generally assumed to be T II. However, since the full laminar T I–T II structure has not been observed in wide tubes and the fully developed state T II has not been measured in narrow tubes, this assumption has not been clearly established. This situation is particularly unfortunate since the wide-tube experiments often involve far more detailed probes of the turbulence than can be employed in narrow tubes. In this paper we provide experimental data from a single tube which bridge the gap between previous wide- and narrow-tube results. Using two complementary experimental techniques we are able for the first time to define the laminar state, state T I, and the full development of state T II in a single flow tube. The results justify the assumption that state T II should be observed in wide tubes, and provide important new information about the nature of states T I and T II and the T I–T II transition.

A typical thermal counterflow apparatus consists of a cell connected by the flow tube to a temperature regulated He II bath as can be seen in Fig. 1. Heat supplied to the cell at a constant rate $\dot{Q}$ produces a steady counterflow of the normal and superfluid components of the He II at an average relative velocity

$$V=\dot{Q}/A\rho_s ST\ , \tag{1}$$

where A is the flow tube area, ρ_s is the superfluid density, T is the ambient temperature, and S is the entropy density. A second heater can be used to generate an additional oscillatory heat flux (amplitude $\delta\dot{Q}$, frequency ω) producing an oscillatory counterflow which is just longitudinal second sound. The geometry of the apparatus is that of a Helmholtz resonator,[1,2] such that the second sound will have a maximum amplitude at a frequency near ω_0 where

$$\omega_0^2=u_2^2A/vl\ . \tag{2}$$

Here u_2 is the speed of second sound, v is the cell volume, and l is the length of the flow tube. At sufficiently low steady velocity V no turbulence is

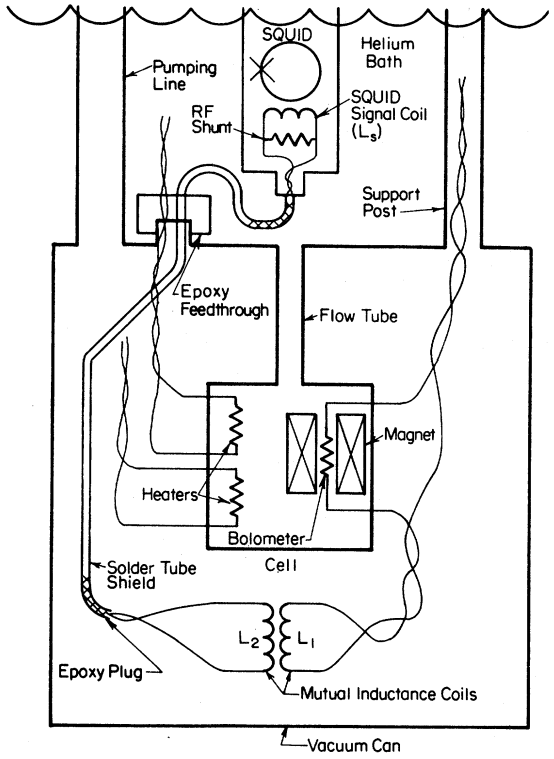

FIG. 1. Schematic diagram of the basic apparatus showing the flow tube connecting the cell to the helium bath, the two heaters, the bolometer and associated magnet, and the SQUID.

present and the only dissipation is provided by the viscosity of the normal fluid. This dissipation gives a simple constant thermal resistance R between the cell and bath, and a temperature difference[3]

$$\Delta T = R\dot{Q} = [128\eta l/\pi d^4 T(\rho S)^2]\dot{Q} \ , \tag{3}$$

where η is the viscosity of the normal fluid. The viscous dissipation also affects a second-sound signal giving a constant width to the resonance curve.

At sufficiently large steady velocity V superfluid turbulence will be present in the flow tube. This turbulence was originally characterized by Vinen[4] as a random distribution of quantized vortex lines having steady-state density L_0. Schwarz[5] has recently shown that a homogeneous turbulent state can be deduced from simple dynamical rules, and has determined L_0 in numerical simulations. The scattering of the normal-fluid excitations from the vortex lines gives rise to an excess dissipation known as mutual friction. The mutual friction force density F_{sn} is related to the line density L_0 by

$$F_{sn} = B\rho_s\rho_n\kappa V L_0/3\rho \ , \tag{4}$$

where B is a dimensionless coefficient related to the vortex line-excitation scattering and measured in several experiments,[6–8] κ is the quantum of circulation, and ρ_s, ρ_n, and ρ are the superfluid, normal-fluid, and total-fluid density, respectively. The excess dissipation provided by F_{sn} can be observed as a temperature difference in excess of that given by Eq. (2) and related to F_{sn} as

$$\Delta T' = lF_{sn}/\rho_s S \ . \tag{5}$$

Similarly, F_{sn} can be observed as a broadening of the second-sound Helmholtz resonance.

Measurements of $\Delta T'$ in narrow tubes[9–13] have revealed that superfluid turbulence evolves through three stages as V is increased. For V less than a critical value V_{c1} only viscous dissipation is observed and $L_0 = 0$. This laminar flow can persist metastably for $V > V_{c1}$, but the stable steady state of the system here is the superfluid turbulent state T I. In this state the line density is given by[3]

$$L_0^{1/2}(\text{T I}) = \gamma_1(T)V - 1.48\alpha_1/d \ , \tag{6}$$

where $\gamma_1(T)$ is a function of temperature, and α_1 is a dimensionless quanity of order unity. At the critical velocity V_{c1} the dimensionless number $L_0^{1/2}d$ is found to be nearly 2.5, independent of temperature and tube size.[14] Above a second critical velocity V_{c2}, where $L_0^{1/2}d$ is approximately 10, the superfluid turbulence makes the transition to state T II. Just above V_{c2} the vortex-line density appears to develop a component in addition to T I [Eq. (6)] such that[10]

$$L_0^{1/2} = L_0^{1/2}(\text{T I}) + \Delta L_0^{1/2} \ , \tag{7}$$

where ΔL_0 varies as $[(V/V_{c2}) - 1]$. For V rather larger than V_{c2} the state T II appears to become fully developed in the sense that the vortex-line density seems to approach an asymptotic form similar to that for state T I,

$$L_0^{1/2}(\text{T II}) \rightarrow \gamma_2(T)V - 1.48\alpha_2/d \ , \tag{8}$$

where the coefficient $\gamma_2(T)$ is roughly twice $\gamma_1(T)$.

The purpose of the present experiments was to determine whether the features of superfluid turbulence observed in these narrow tubes persist in tubes an order of magnitude larger. No single experimental technique can span the range of low-level dissipation presented by this situation. In a tube of 10^{-1} cm diameter, for example, the temperature difference would vary from about 10^{-7} K in laminar flow to about 10^{-4} K in the fully developed T II superfluid turbulent state. Instead we have employed two techniques. To determine the laminar and superfluid turbulent state T I we have measured the attenuation of second-sound Helmholtz oscillations. Above V_{c2} these oscillations become overdamped, and we have used a measurement of the dynamic thermal resistance to determine state T II.

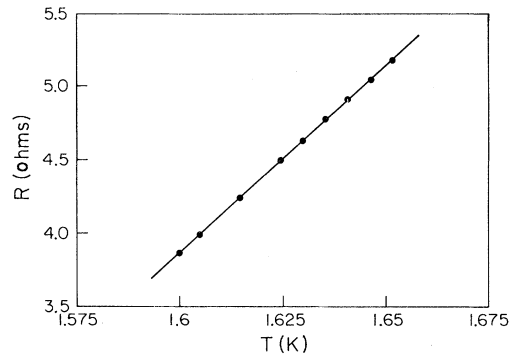

FIG. 2. Calibration curve for the bolometer at 1.6 K. Solid line corresponds to $(1/R_b)(dR_b/dT)=6.9\ \mathrm{K}^{-1}$.

APPARATUS

The apparatus is shown schematically in Fig. 1. The flow tube was glass with an inside diameter of $(1\pm0.01)\times10^{-1}$ cm and a length of 10 cm. In the worst case the normal-fluid laminar entrance length was only a few diameters.[15] The cell was machined from cast epoxy[16] and contained two heaters, a superconducting bolometer and an associated magnet, and had a free volume of 5.03 cm^3. The superconducting leads for the magnet, secondary inductance coil (L_2), and heaters all passed out of the vacuum can through an epoxy seal, and the leads for the bolometer and primary inductance coil (L_1) were passed through a support tube to a room-temperature seal.

The bolometer was a superconducting thin film made from 95-at.% Sn and 5-at.% In alloy[17] evaporated onto a glass substrate. A film of this alloy at zero magnetic field has a sharp resistive transition at about 3.5 K. At finite fields the transition is broadened and shifted to lower temperature. For the three temperatures studied in this experiment (1.5, 1.6, and 1.7 K) a field of about 600 G was sufficient to put the center of the transition at the desired temperature. Figure 2 shows the bolometer calibration curve at 1.6 K, with the straight line corresponding to $(1/R_b)(dR_b/dT)=6.9\ \mathrm{K}^{-1}$. The thermal response time of the bolometer was less than 1 ms.

The magnetic field used to shift the transition of the bolometer was produced by a superconducting persistent-current solenoid. The solenoid was wound of 1980 turns of NbTi wire on a tubular epoxy former, and the bolometer was secured in the center of the bore. A persistent-current mode could be established with a thermal switch in the He bath.

The bolometer was coupled to the superconducting quantum-interference device (SQUID) (Ref. 18) pickup coil (L_s) by two inductance loops (L_1 and L_2) wound of superconducting wire and surrounded by a lead shield. The values of L_1 and L_2 were chosen to maximize the signal coupled into the SQUID. The leads of L_2 were shielded by a superconducting tube. An rf shunt placed across L_2 (a 3.5-mm piece of Manganin wire with a resistance of 0.12 Ω) reduced the rf noise coupled into the SQUID (3-dB rolloff at 20 kHz). The effective mutual inductance M_{eff} between L_1 and L_s was measured[19] to be 0.62 μH.

The bolometer was the single detector used in both the second-sound and thermal-resistance measurements. It was biased by a constant voltage V_b of about 150 mV from a specially constructed[19] temperature-stabilized dc voltage supply of low-noise (<1 μV), long-term stability (<10 μV/h), and low-output impedance R_0. The output voltage of the SQUID detector system dV resulting from a change in cell temperature dT was then

$$dV=\frac{(20\ \mathrm{mV})}{\phi_0}M_{\mathrm{eff}}\frac{V_b}{R^2}\frac{dR_B}{dT}dT\ , \tag{9}$$

where ϕ is the flux quantum (2×10^{-15} Wb/m^2) and R is the total resistance in the circuit composed of R_0, R_b, and the lead resistance R_L. With the use of

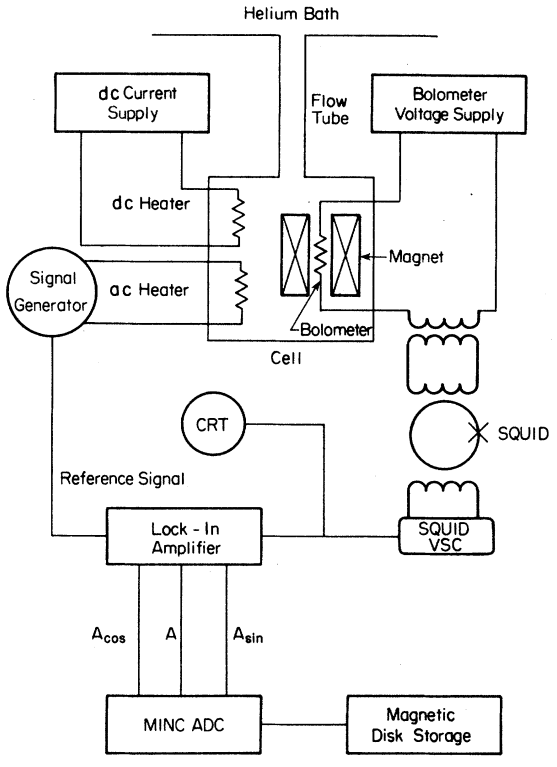

FIG. 3. Schematic diagram of the experimental configuration used in the second-sound—attenuation measurements.

the measured circuit parameters, a temperature change dT of 1 μK gives an output voltage of about 2.5 mV.

RESULTS

To determine the laminar and low—line-density state T I the attenuation of second-sound Helmholtz oscillations was measured as a function of the dc heat current $\dot{Q}$ or the constant relative velocity V [Eq. (1)]. The experimental configuration is shown in Fig. 3. A sinusoidal heat current of 30-μW amplitude and frequency $\omega/2$ was generated by the ac heater, and the temperature oscillations at frequency ω in the cell $\Delta T(\omega)$ were detected by the bolometer-SQUID system. The maximum amplitude of these oscillations was about 1.5 μK. The SQUID output was detected by a lock-in amplifier, and the in-phase, out-of-phase, and vector sum were digitized and stored by the MINC computer at a rate of four samples per second. Up to 100 samples were required to determine the second-sound amplitude $\Delta T(\omega)$, and this was repeated at various frequencies between 1 and 10 Hz. Sample-resonance curves obtained at 1.7 K are shown in Fig. 4. These results show that the second-sound attenuation remains constant as V is increased until the superfluid turbulent state T I appears above about 1 cm/s. For velocities greater than about 2 cm/s the damping is too large for this technique to be useful.

With the use of the standard two-fluid hydrodynamic equations including the mutual friction force (see Appendix) it follows that the second-sound amplitude $\Delta T(\omega)$ is given by

$$\Delta T(\omega)=\frac{\Delta\dot{Q}}{C}\left[\frac{(\Omega_1^2-\Omega_3^2)\Omega_2+i(\Omega_3^2\Omega_1^2/\omega-\omega\Omega_2^2)}{\Omega_1^4+\omega^2\Omega_2^2}\right], \tag{10}$$

where $\Delta\dot{Q}$ is the amplitude of the ac heat flux, C is the heat capacity of the helium in the cell, and

$$\Omega_1^2=\omega_0^2-\omega^2[1-(\rho_s/\rho)(\delta/a)], \tag{11}$$

$$\Omega_2=\omega(\rho_s/\rho)(\delta/a)-\kappa L_0 B/3, \tag{12}$$

$$\Omega_3^2=\omega^2[1-(\rho_s/\rho)(\delta/a)]. \tag{13}$$

The normal-fluid viscosity η enters these expressions through the penetration length δ, where

$$\delta^2=2\eta/\omega\rho_n, \tag{14}$$

and the vortex line density only appears in Ω_2. The experimental data were fit to the magnitude of $\Delta T(\omega)$ computed from Eq. (10) using ω_0 and L_0 as parameters. The resonant frequency $\omega_0/2\pi$ was found to be 3.76±0.02 Hz essentially independent of temperature and counterflow velocity V. This result compares quite favorably with the value 3.87 Hz calculated from Eq. (2) using measured values of the cell and flow-tube dimensions. The solid lines in Fig. 4 are drawn with the optimum values of the vortex-line density L_0 and illustrate the excellent fit to the data. The values of the line density determined from this procedure at 1.7 K are collected in Fig. 5(c), where the dimensionless quantity $L_0^{1/2}d$ is given as a function of the relative velocity V. Similar data obtained at 1.5 and 1.6 K are given in Figs. 5(a) and 5(b), respectively.

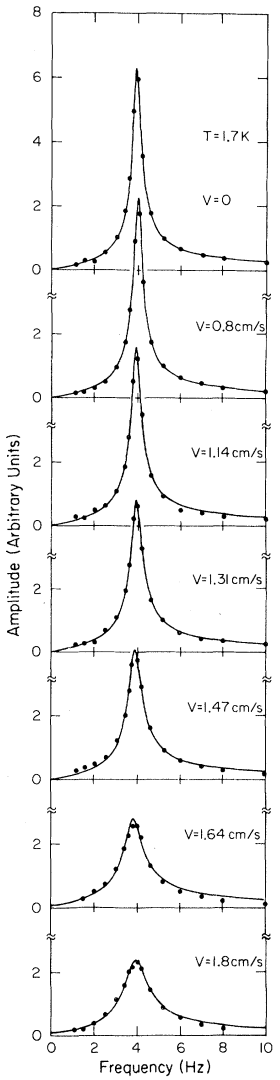

FIG. 4. Example second-sound Helmholtz resonance curves at 1.7 K, and at the velocities indicated. Solid lines are best fits of Eq. (10) to the data using the vortex-line density as a parameter.

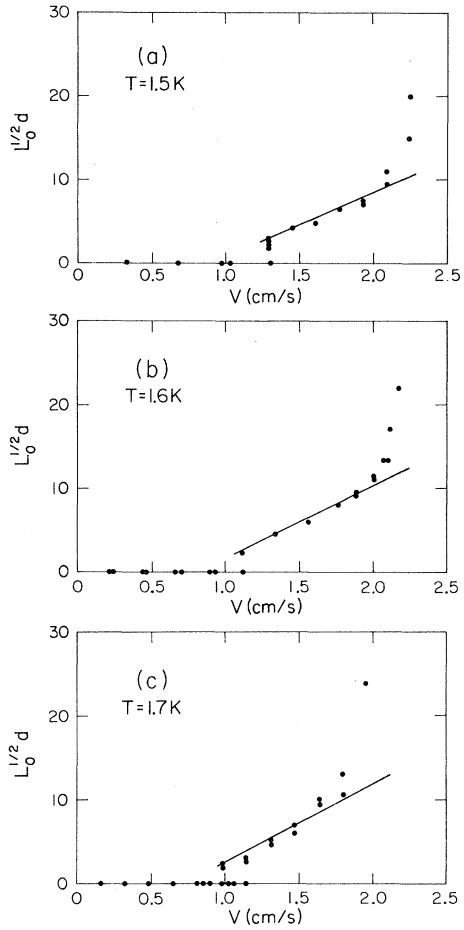

FIG. 5. Vortex-line density, shown as the dimensionless number $L_0^{1/2}d$, as a function of the velocity V at 1.5, 1.6, and 1.7 K. Solid lines are best fits of Eq. (6) to the data. Parameters $\gamma_1(T)$ and α_1 are given in Table I.

Although these results will be discussed in detail below, it should be noted here that the laminar ($L_0=0$) state and the superfluid turbulent state T I are clearly defined in these data. Indeed at 1.7 K there is evidence of the metastable laminar state above 1 cm/s. At the largest velocities L_0 has increased to the point that the second sound is severely damped and it is no longer a useful probe of the superfluid turbulence.

In order to determine the vortex-line density in state T II at higher velocities we have employed a heat-pulse technique[10] to measure the dynamic thermal resistance of the turbulent counterflow. A steady heat current $\dot{Q}$ produces a steady temperature difference ΔT, and the dynamic thermal resistance is defined as

$$R(\dot{Q})=\frac{d\Delta T}{d\dot{Q}} . \tag{15}$$

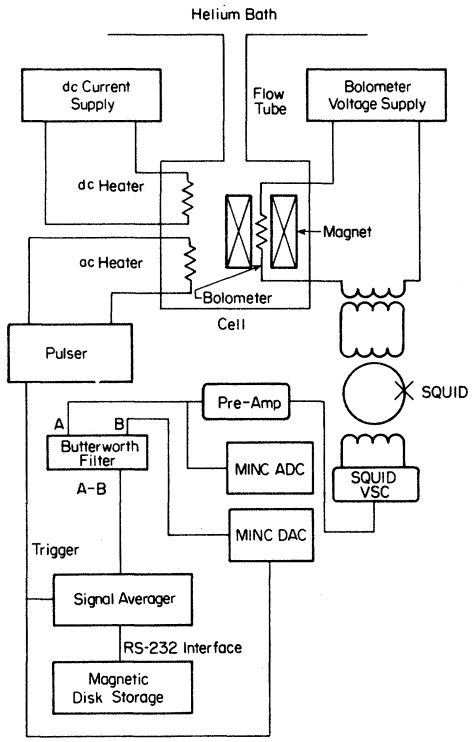

FIG. 6. Schematic diagram of the experimental configuration used in the heat-pulse measurements.

It follows that if the heat current is increased by $\delta\dot{Q}$ then ΔT will increase by

$$\delta T_0=R(\dot{Q})\delta\dot{Q} . \tag{16}$$

In laminar counterflow the thermal resistance is constant [Eq. (3)] and is determined by the normal-fluid viscosity. In turbulent counterflow the mutual friction force increases the thermal resistance and produces a nonlinear dependence of R on the heat current $\dot{Q}$.

The experimental configuration used to measure the thermal resistance is shown in Fig. 6. A constant temperature difference ΔT was established with the dc heater. Square voltage pulses applied to the ac heater generated heat pulses of amplitude $\delta\dot{Q}$ between 50 and 100 μW. Following the application of a pulse, the cell temperature increased with time reaching a steady value $\Delta T+\delta T_0$. The width and spacing of the $\delta\dot{Q}$ pulses were long enough so that the temperature of the cell reached steady values on both the rise and fall. The temperature of the cell was detected by the bolometer-SQUID system discussed above. The SQUID output signal was amplified and filtered (dc to 15 Hz) before going to a digital signal averager. A trigger from the pulser preceded each pulse and started the averager on a signal

sweep. The sweep time was set so that a complete temperature rise and fall and an adequate baseline could be recorded in one sweep. At the largest heat currents, when δT_0 was as large as 0.1 mK, as few as 75 sweeps were adequate to resolve the temperature signal. At the other extreme, several hundred sweeps were required. Since the signal averager could only digitize positive voltages within a (0—1) window, a voltage offset B was subtracted from the preamplifier output A so the signal arriving at the averager was within this window. Bath drift and bolometer-voltage drift caused the signal to shift so the compensating voltage was reset before each sweep. The amount of offset B sent into the filter was determined by averaging the output of the preamplifier during one sweep with the computer which then calculated the offset needed to keep the signal in the (0—1)-V window. This voltage was then supplied during the next sweep.

The temperature signals produced by the heat pulses and recorded on the signal averager took two different forms. When the steady heat current $\dot{Q}$ was small, in the region of the second-sound attenuation data, the signal appeared like the example in Fig. 7. A second-sound "ringing" appeared at the start and finish of the heat pulse. The frequency was equal to ω_0 [Eq. (2)] within the considerable error, and the attenuation was due to the normal-fluid viscosity and the mutual friction just as for the driven oscillations.

Although these data with the second-sound ringing do indicate a steady-state temperature difference δT_0, the data are really at the limit of resolution for this heat-pulse technique. The signal shown in Fig. 7, for example, required 698 sweeps to barely resolve

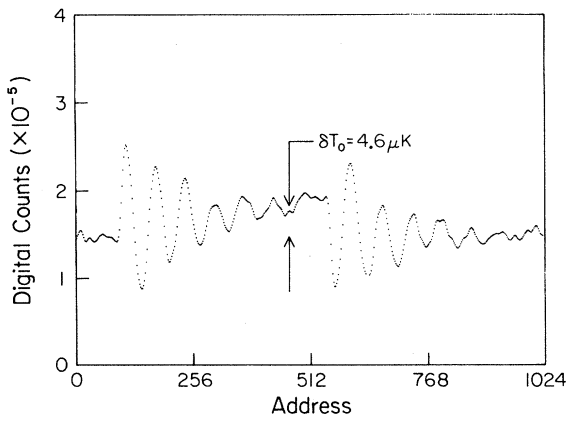

FIG. 7. Example of second-sound ringing response to a heat pulse when the turbulence was in state T I. Vertical scale is proportional to the temperature difference and horizontal scale is proportional to the time. Steady temperature difference δT_0 of 4.6 μK is shown.

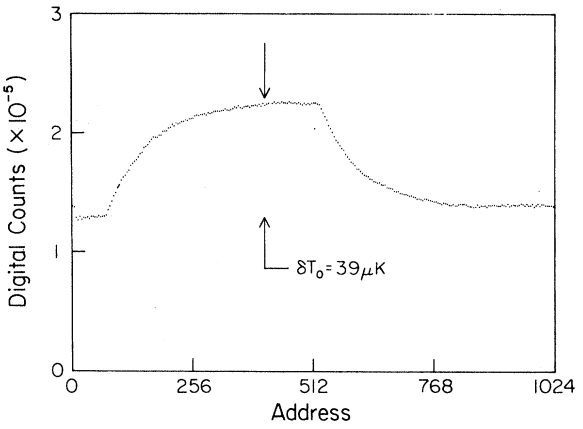

FIG. 8. Example of exponential response to a heat pulse when the turbulence was in state T II. Vertical scale is proportional to temperature and horizontal scale is proportional to time. Steady temperature difference of 39 μK is shown.

the temperature difference of 4.6 μK. Not surprisingly, the values of the thermal resistance obtained from such data showed considerable scatter. The results were not inconsistent with the vortex-line density obtained from the second-sound—resonance measurements, however. The second-sound—resonance technique is clearly superior in this low—heat-current, low—vortex-line-density region of the turbulence.

The second form of temperature signal produced by the heat pulses occurred when the steady heat current $\dot{Q}$ was greater than that needed to provide critical damping of the second-sound resonance. A typical signal shown in Fig. 8 has an exponential rise of the temperature to δT_0 and an exponential fall when the pulse is removed. The time constant τ of the exponential is of course just $R(\dot{Q})C$, where C is the heat capacity of the helium in the cell. The thermal resistance $R(\dot{Q})$ can thus be obtained from such a signal both from the time constant τ and the amplitude δT_0. The system parameters are so arranged that the heat-pulse technique begins to generate these exponential signals just as the second-sound—resonance technique is becoming ineffective. In this sense the two techniques are overlapping and complementary.

After correcting for small baseline slant due to drift in the bath temperature or the bolometer voltage, the temperature signals were fit to a simple exponential rise and decay with amplitude δT_0 and time constant τ. Calibration of the signal amplitude in K was made possible by using the absolute value of $R(\dot{Q})$ obtained from the time constant τ. Figure 9 shows the thermal resistance as a function of the steady heat current $\dot{Q}$ at 1.7 K. At low heat

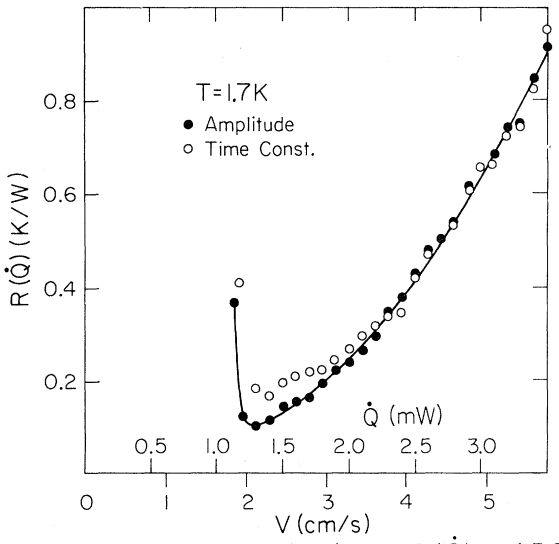

FIG. 9. Dynamic thermal resistance $R(\dot{Q})$ at 1.7 K determined from amplitude (δT_0) and time-constant (τ) measurements as a function of the heat current $\dot{Q}$ and velocity V. Systematic difference at low velocity is suggestive of an intrinsic relaxation time of the turbulence. Solid line drawn through the amplitude data is used to calculate $\Delta T(\dot{Q})$ using Eq. (17).

currents the ringing signal (Fig. 7) rather than the exponential signal is observed. The results obtained from both the amplitude δT_0 and time constant τ are distinguished in the figure and are seen to be in excellent agreement at the larger heat currents. Near the lowest heat current at which an exponential signal is observed, there is a systematic deviation of the time-constant and amplitude data. We interpret this as evidence for an intrinsic relaxation time of the vortex-line distribution that is becoming very large near the T I—T II transition. Such a relaxation time would be consistent with Vinen's waiting-time measurements[20] and could reveal an important feature of the transition.

The vortex-line density L_0 was extracted from the dynamic thermal-resistance data by first fitting a smooth function to the $R(\dot{Q})$ data obtained from the signal amplitude δT_0. The functional fit to the 1.7-K data is shown by the line in Fig. 9. A numerical integration of $R(\dot{Q})$ was then performed to give $\Delta T(\dot{Q})$,

$$\Delta T(\dot{Q})=\Delta T(\dot{Q}_0)+\int_{\dot{Q}_0}^{\dot{Q}} R(\dot{Q})d\dot{Q} \ . \qquad (17)$$

The starting point for the integration $\dot{Q}_0$ was in the region of overlap with the second-sound data. The constant of integration $\Delta T(\dot{Q}_0)$ was calculated from the vortex-line density at $\dot{Q}_0$ determined by the second-sound technique. The vortex-line density L_0 could then be calculated from $\Delta T(\dot{Q})$ using Eqs.

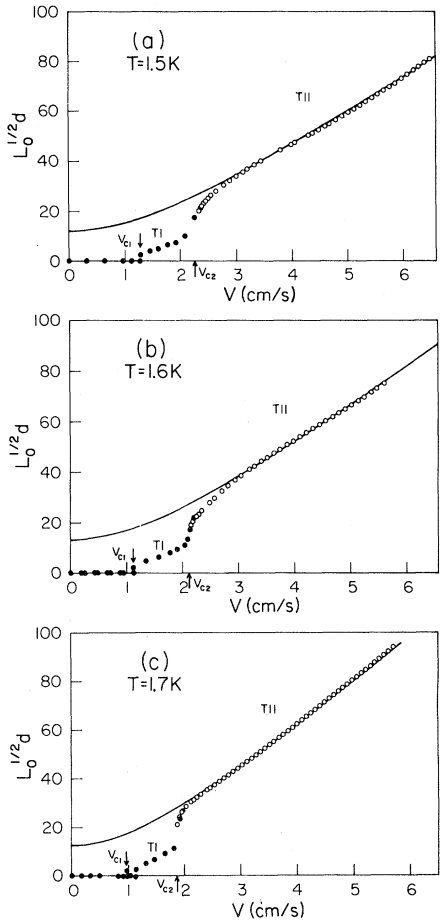

FIG. 10. Vortex-line density, shown as the dimensionless number $L_0^{1/2}d$, as a function of velocity V at 1.5, 1.6, and 1.7 K. Open circles are determined from the heat-pulse measurements and are representative of state T II. Solid circles are taken from the second-sound measurements of state T I shown in Fig. 5. Critical velocities V_{c1} and V_{c2} are indicated. Solid line is a best fit of Eq. (18) to the state T II data, with the parameters given in Table I.

(4) and (5) since the temperature difference from the laminar flow [Eq. (3)] is entirely negligible here. The results for the line density obtained from the dynamic thermal-resistance measurements and characteristic of state T II are shown as the dimensionless number $L_0^{1/2}d$ in Fig. 10. Reasonable variations of the curve fit to the $R(\dot{Q})$ data or of the choice of $\dot{Q}_0$ in the integration had virtually no effect on the resulting line density. Also included in Fig. 10 are the results for the line density in state T I obtained from the second-sound measurements (Fig. 5). The combined results give a very complete picture of the evolution of superfluid turbulence in this wide tube.

ANALYSIS

The fundamental question addressed by these experiments is clearly answered by the results shown in Fig. 10. The basic evolution of superfluid turbulence from the laminar ($L_0=0$) state through states T I and T II appears precisely as in circular tubes an order of magnitude smaller. The analysis of these states and of the critical velocities V_{c1} and V_{c2} gives no reason to suppose that a similar evolution does not proceed in tubes of any larger size. Brewer and Edwards[12] have reported measurements of the temperature difference in circular tubes of three different sizes (0.005, 0.011, and 0.037 cm) which are completely consistent with this conclusion. The present results are the first to show the evolution of superfluid turbulence in a single tube with an accurate definition of each state.

The vortex-line density in state T I as given by the second-sound attenuation data is shown in Fig. 5. The straight lines are fits of Eq. (6), and the values of $\gamma_1(T)$ and α_1 are given in Table I. The results for $\gamma_1(T)$ are in good agreement with the data of Childers[9] in tubes of sizes an order of magnitude smaller. Other experiments which have observed this state are less precise but are quite consistent with the present data. The dimensionless quantity α_1 is approximately 5 in these wide-tube experiments. This is consistent with the observation of Ladner[21] that α_1 is a weakly increasing function of tube diameter. It is worth recalling at this point that in pure superflow, where the turbulence is apparently homogeneous, the quantity α is zero.[22,23] It seems likely that this quantity is related to an inhomogeneity in the turbulence produced by the normal-fluid flow.

The transition from laminar ($L_0=0$) flow to state T I is not determined with great precision in these experiments, although this is by far the widest tube in which the transition has ever been observed. The smallest stable line density which could be observed was fully consistent with the critical condition $L_0^{1/2}d=2.5$ found in a variety of narrow-tube experiments.[14] If the turbulence in state T I were homogeneous, this critical condition would correspond to an average vortex-line spacing of only $d/2.5$.

TABLE I. Experimental values of the parameters in Eqs. (6) and (18).

T (K)	1.5	1.6	1.7
γ_1 (s/cm^2)	77	86	92
α_1	5.1	4.7	5.0
γ_2 (s/cm^2)	145	163	190
C	31	33	33
α_2	13	14	14

The vortex-line density in state T II shown in Fig. 10 does appear to reach an asymptotic limit as given by Eq. (8), but only for $V>2V_{c2}$. We have found that the line density is well described over a much wider domain by the function

$$L_0^{1/2}d=\{[\gamma_2(T)Vd]^2+C^2\}^{1/2}-1.48\alpha_2\,, \qquad (18)$$

which, of course, has the same asymptotic form as Eq. (8). The solid lines in Fig. 10 are obtained from Eq. (18) using the values for $\gamma_2(T)$, α_2, and C given in Table I. The temperature-difference data of Chase[24] (0.08-cm tube) and Brewer and Edwards[12] (0.037-cm tube) can also be very well described by the line density given by Eq. (18). In Fig. 11 we show the temperature dependence of the quantity $\gamma_2(T)$ determined from the present experiment. Also shown is a collection of other data[12,24–26] from circular tubes which is unquestionably representative of asymptotic state T II. The overall agreement must be considered rather good considering the variety of experiments.

A significant and revealing feature of the data in Fig. 11 is the agreement with the calculation of Schwarz[5] shown by the solid line. The Schwarz theory describes homogeneous turbulence, observed experimentally in pure superflow,[22,23] and it is therefore somewhat surprising to find this agreement. Of course the vortex-line density in superflow has $\alpha=0$, and so the agreement is not complete. There is a clear implication, however, that fully developed superfluid turbulence in state T II is reasonably homo-

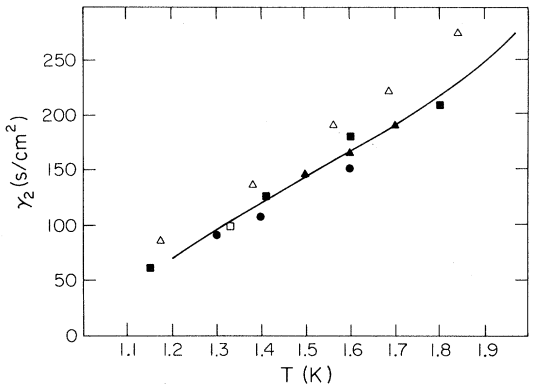

FIG. 11. When state T II is fully developed, the vortex-line density is given by the asymptotic form in Eq. (8). Amplitude $\gamma_2(T)$ is shown here as a function of temperature determined from the present experiment (▲) and from the following previous experiments: ●, Dimotakis and Broadwell (Ref. 25, $d=0.318$ cm); □, Peshkov and Tkachenko (Ref. 26, $d=0.274$ cm); △, Brewer and Edwards (Ref. 12, $d=0.037$ cm); and ■, Chase (Ref. 24, $d=0.08$ cm). Solid line is the calculation of Schwarz (Ref. 5) for homogeneous turbulence.

geneous. Thermal counterflow in high—aspect-ratio rectangular tubes[7,27] (approximately a parallel-plate geometry) exhibits only a single superfluid turbulent state (T III) with a temperature coefficient $\gamma_3(T)$ quite comparable to $\gamma_2(T)$. We have previously suggested[27] that the states T I and T III are equivalent and that $\gamma_3/\gamma_1 = D/d$, where D is the hydraulic diameter [4×(area)/(perimeter)] of the tube. The present results, when compared to pure superflow, suggest the alternative possibility that T II and T III may be equivalent, approximately homogeneous states, and the low—line-density state T I is inhomogenous.

The functional form for the line density in state T II given by Eq. (18) fails to describe the data in the neighborhood of the transition to state T I at V_{c2}. A line density of the form found in narrow tubes[10] and given by Eq. (7) can be fit to the data, although a somewhat weaker power law like $[(V/V_{c2})-1]^{2/3}$ appears to give a better fit. The very rapid change of L_0 with V near V_{c2} is of course the reason for the thermal-resistance peak here (Fig. 9), as observed earlier in narrow tubes.[10] It is worth noting again that the time-constant data suggest a characteristic relaxation time for the line density that is divergent near V_{c2}.

We have somewhat arbitrarily defined the critical velocity V_{c2} marking the transition from state T I to T II to correspond with the peak in the thermal-resistance data. In fact, since the transition region is quite narrow, there is little error introduced by this choice. Comparison of the present V_{c2} data with results from narrow tubes indicates a roughly $1/d$ dependence, and consequently we have plotted our results in Fig. 12 as $V_{c2}d$. This procedure does not eliminate all of the size dependence, however. The present results compare quite well with those of Chase[24] obtained in a tube of nearly the same size (0.08 cm) whereas the results from both Ladner *et al.*[10] and Brewer and Edwards[12] obtained from comparable-size tubes an order of magnitude smaller are systematically lower. We conclude that V_{c2} is a weak function of both temperature and tube size. It is tempting to relate this weak size dependence to that of α_1, and this can easily be done by setting the critical condition to be that the vortex-line density in state T I reaches some constant value L_{c1} at the transition. It then follows from Eq. (6) that

$$V_{c2}d = (L_{c1}^{1/2}d + 1.48\alpha_1)/\gamma_1(T) \ . \tag{19}$$

The lines in Fig. 12 are calculated from Eq. (19) using $\alpha_1 = 5$ for the wide tubes and $\alpha_1 = 1$ for the narrow ones and with $L_{c1}^{1/2}d = 10$. The agreement with the data is somewhat encouraging, especially as the magnitude of the size dependence is approximately correct.

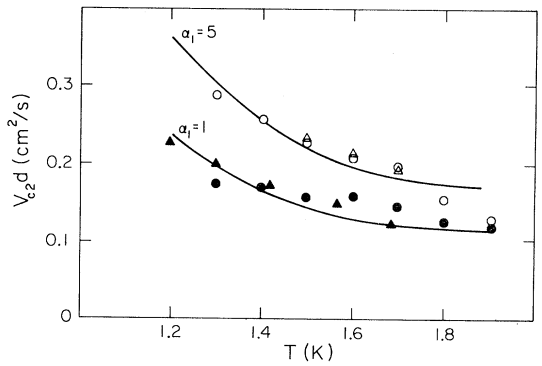

FIG. 12. Second critical velocity at the transition between state T I and T II. Results are shown for two wide tubes: △, the present experiment ($d = 0.10$ cm), and ○, Chase (Ref. 24, $d = 0.08$ cm); and two tubes an order of magnitude narrower: ▲, Brewer and Edwards (Ref. 12, $d = 0.011$ cm), and ●, Ladner *et al.* (Ref. 10, $d = 0.013$ cm). Size dependence is largely but not completely removed by plotting $V_{c2}d$. Solid lines are calculated from Eq. (19) using a critical state T I line density $L_{c1}^{1/2}d = 10$, and the values of α_1 noted in the figure and appropriate to the wide and narrow tubes.

CONCLUSIONS

Using two complementary techniques we have determined the evolution of superfluid turbulence in thermal counterflow in a single wide circular tube through the laminar ($L_0 = 0$) state and the states T I and T II. We have demonstrated that this evolution is qualitatively the same as in tubes an order of magnitude narrower and quite likely is a generic feature of the circular geometry. The parameters of states T I and T II are in excellent quantitative agreement with previous data, and suggest that the fully developed T II state is reasonably homogeneous. Associated with the T I—T II transition is an intrinsic relaxation time for the vortex-line density that appears to diverge at V_{c2}. The concept of a critical line density which seems to be correct at V_{c1} may also be appropriate for V_{c2}. Further experiments will be needed to clarify the nature of this transition, and of the states T I and T II.

It has been recently recognized that superfluid turbulence in thermal counterflow is strongly influenced by tube geometry.[27] Our present results show that for the circular geometry tube size has no qualitative effect on the evolution of the turbulence, and only a weak quantitative effect on state T I and on the transition to T II at V_{c2}. Similar conclusions can be drawn in the case of the parallel-plate geometry. Here only the single state T III is observed in both wide[7] and narrow[27] tubes, and the

line-density coefficient $\gamma_3(T)$ is independent of tube size. The square geometry has also been studied in both wide and narrow tubes, but in this case the tube-size independence has not been established. In narrow square tubes, Henberger and Tough[28] found an evolution of the turbulence quite similar to that in the circular geometry. In state T I the parameters $\gamma_1(T)$ and α_1 are found to be in agreement with the circular-tube results. The critical velocity V_{c2} was less reproducible and was somewhat lower than in the circular tubes.[29] Because of the large temperature difference the full development of state T II could not be determined. In a wide square tube, however, Barenghi *et al.*[30] found only a single superfluid turbulent state. The properties of this state were in fair agreement with the results for state T I. This is particularly surprising since the experiment is limited to rather high velocities where $L_0^{1/2}d > 25$. It may be appropriate here to note the original experiments of Vinen[31] which involved wide, low—aspect-ratio rectangular tubes. Like the experiments in small square tubes, Vinen's results also indicated an evolution from a (poorly defined) low—low-density state to a fully developed state consistent with T II. Obviously the evolution of superfluid turbulence is strongly geometry dependent, but in the majority of experiments the qualitative features are independent of the tube size.

ACKNOWLEDGMENT

This work has been supported by National Science Foundation—Low Temperature Physics Grant No. DMR-79-25089.

APPENDIX

As mentioned in the text above, the cell and counterflow channel form a second-sound Helmholtz oscillator.[1,2] In this appendix the frequency response of the resonator and the primary damping mechanisms of the temperature oscillations are calculated. Consider the system shown in Fig. 13 and let there be a dc heat current $\dot{Q}$ from one heater and a small ac heat current $\Delta\dot{Q}(t)$ from the other heater, where

$$\Delta\dot{Q}(t)=\Delta\dot{Q}\,e^{-i\omega t}\,. \tag{A1}$$

These two heat currents generate thermal counterflow through the tube. The axial (z) components of the normal-fluid and superfluid velocities in the tube are written as

$$V_n=V_{n0}(r)+\Delta V_n(r)e^{-i\omega t}\,, \tag{A2}$$

$$V_s=V_{s0}(r)+\Delta V_s(r)e^{-i\omega t}\,, \tag{A3}$$

where $V_{n0}(r)$ and $V_{s0}(r)$ are the time-independent velocities for steady-state counterflow. The ac velocity fields are produced by $\Delta\dot{Q}(t)$.

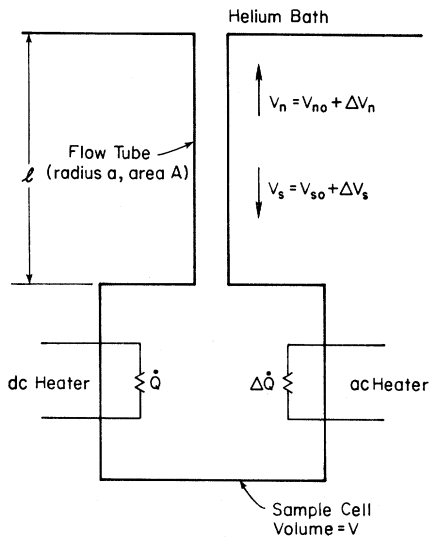

FIG. 13. Schematic diagram of the cell and flow tube used to calculate the frequency response of the second-sound Helmholtz oscillations in the Appendix.

Entrance-length effects appear in a small fraction of channel length and so will be neglected. The wavelengths of second sound at these frequencies are much larger than the dimensions of the cell and flow tube. This allows any $\exp(ikz)$ dependence to be eliminated from Eqs. (A2) and (A3). The temperature oscillations may be assumed to be uniform throughout the cell and equal to the spatial average of the temperature across the cell end of the flow tube.

In the spirit of the mutual-friction approximation[3] we assume that the only velocity fields are axial [Eqs. (A2) and (A3)] in which case the two-fluid equations of motion can be written

$$\rho_n\frac{\partial V_n}{\partial t}=\eta\frac{1}{r}\frac{\partial}{\partial r}\left[r\frac{\partial V_n}{\partial r}\right]-\frac{\rho_n}{\rho}\frac{\partial P}{\partial z}-\rho_s S\frac{\partial T}{\partial z}+F_{sn}\,, \tag{A4}$$

$$\rho_s\frac{\partial V_s}{\partial t}=\frac{\rho_s}{\rho}\frac{\partial P}{\partial z}+\rho_s S\frac{\partial T}{\partial z}-F_{sn}\,, \tag{A5}$$

where F_{sn} is the axial component of the mutual-friction force. Substituting Eqs. (A2) and (A3) into Eqs. (A5) and (A6), and keeping only terms linear in $\Delta V_n(r)$ and $\Delta V_s(r)$, and averaging over the tube cross section leads directly to

$$-i\omega\,\Delta V_n e^{-i\omega t}=G-\frac{1}{\rho}\frac{\Delta P}{l}-\frac{\rho_s}{\rho_n}S\frac{\Delta T}{l}+\frac{F_{sn}}{\rho_n}\,, \tag{A6}$$

$$-i\omega \Delta V_s e^{-i\omega t} = -\frac{1}{\rho}\frac{\Delta P}{l} - S\frac{\Delta T}{l} - \frac{F_{sn}}{\rho_s} , \tag{A7}$$

where ΔP and ΔT are the total pressure and temperature difference along the tube and G is the average of the viscosity term,

$$G = \frac{\eta}{\rho_n}\int_0^a \left[\frac{1}{r}\frac{\partial}{\partial r}\left[r\frac{\partial V_n}{\partial r}\right]\right]\frac{2\pi r}{A}dr . \tag{A8}$$

Subtracting Eqs. (A6) and (A7) gives

$$-i\omega(\Delta V_n - \Delta V_s)e^{-i\omega t} = G - \frac{\rho S}{\rho_n}\frac{\Delta T}{l} + \frac{\rho}{\rho_s \rho_n}F_{sn} . \tag{A9}$$

We now write the relative velocity V, the temperature difference ΔT, and the mutual friction force F_{sn} in terms of their dc values V_0, T_0, and F_{sn0} as

$$V = V_0 + \Delta V e^{-i\omega t} , \tag{A10}$$

$$\Delta T = \Delta T_0 + \Delta T(\omega)e^{-i\omega t} , \tag{A11}$$

$$F_{sn} = F_{sn0} + \Delta F_{sn} e^{-i\omega t} , \tag{A12}$$

where

$$\Delta F_{sn} = \frac{\kappa B \rho_s \rho_n}{3\rho} L_0 \Delta V \tag{A13}$$

follows from Eq. (4). Combining Eqs. (A9)–(A12) gives then

$$-i\omega(\Delta V_n - \Delta V_s) = G - \frac{\rho S}{\rho_n l}\Delta T(\omega) + \frac{\rho}{\rho_n \rho_s}\Delta F_{sn} . \tag{A14}$$

The use of the thermal counterflow condition,

$$\rho_n \Delta V_n = -\rho_s \Delta V_s \tag{A15}$$

and Eq. (A13) in Eq. (A14), then gives

$$\Delta T(\omega) = \frac{\rho_n l}{\rho S}[(i\omega + B\kappa L_0/3)(\rho/\rho_s)\Delta V_n + G] . \tag{A16}$$

We compute the viscosity term G using a boundary-layer form[32] for $\Delta V_n(r)$,

$$\Delta V_n(r) = \Delta V_n\{1 - \exp[-(1+i)(a-r)/\delta]\} , \tag{A17}$$

where the viscous penetration depth δ is given by

$$\delta^2 = 2\eta/\omega\rho_n . \tag{A18}$$

This approximation is strictly valid for $\delta/a \ll 1$. In the worst case for the present experiment $\delta/a \simeq 0.2$ and our calculation can only be considered correct to first order in δ/a. A general solution for the oscillatory viscous flow in a tube has been given by Uchida.[33] We have considered higher-order terms in the solution, but the effect is negligible. With the use of Eq. (A17), the straightforward evaluation of G gives

$$G = -\omega \Delta V_n (1+i)\delta/a . \tag{A19}$$

Combining this result with Eq. (A16) gives

$$\Delta T(\omega) = \frac{\rho_n l}{\rho_s S}[(i\omega + \gamma)(\rho/\rho_s) - \omega(1+i)\delta/a]\Delta V_n , \tag{A20}$$

where

$$\gamma \equiv \kappa B L_0/3 . \tag{A21}$$

Finally it is necessary to consider the energy balance of the system. Heat is supplied to the cell at a rate $\Delta\dot{Q}$, is conducted along the flow tube at a rate $\Delta\dot{Q}_t$, and heats the cell at a rate $\Delta\dot{Q}_c$. Thus

$$\Delta\dot{Q} = \Delta\dot{Q}_t + \Delta\dot{Q}_c , \tag{A22}$$

where

$$\Delta\dot{Q}_t = \rho S T \Delta V_n A \tag{A23}$$

and

$$\Delta\dot{Q}_c = i\omega C \Delta T(\omega) . \tag{A24}$$

Combining Eqs. (A20)–(A24) leads eventually to the desired result for the frequency dependence of the temperature oscillation amplitude,

$$\Delta T(\omega) = \frac{\Delta\dot{Q}}{C}\frac{[(\Omega_1^2 - \Omega_3^2)\Omega_2 + i(\Omega_3^2\Omega_1^2/\omega - \omega\Omega_2^2)]}{\Omega_1^4 + \omega^2\Omega_2^2} , \tag{A25}$$

where

$$\Omega_1^2 = \omega_0^2 - \omega^2(1-\epsilon) , \tag{A26}$$

$$\Omega_2 = \omega\epsilon - \gamma , \tag{A27}$$

$$\Omega_3^2 = \omega^2(1-\epsilon) , \tag{A28}$$

$$\epsilon = (\rho_s/\rho)(\delta/a) . \tag{A29}$$

The resonant frequency is as given by Eq. (2),

$$\omega_0^2 = u_2^2(A/vl) , \tag{A30}$$

where the second-sound velocity is[32]

$$u_2^2 = S^2 T(\rho_s/\rho_n)/(C/\rho v) . \tag{A31}$$

*Present address: Department of Physics, Boston University, Boston, MA 20115.

[1]H. C. Kramers, T. M. Wirada, and A. Broese van Groenou, in *Proceedings of the VIIth International Conference on Low Temperature Physics,* edited by G. M. Graham and A. C. Hollis-Hallett (North-Holland, Amsterdam, 1960), p. 23.

[2]M. Kriss and I. Rudnick, Phys. Rev. 174, 326 (1968).

[3]J. T. Tough, in *Progress in Low Temperature Physics,* edited by D. F. Brewer (North-Holland, Amsterdam, 1982), Vol. VIII, Chap. 3.

[4]W. F. Vinen, Proc. R. Soc. London Ser. A 242 (1957).

[5]K. W. Schwarz, Phys. Rev. Lett. 38, 551 (1977); Phys. Rev. B 18, 245 (1978); Phys. Rev. Lett. 49, 283 (1982).

[6]P. Lucas, J. Phys. C 3, 1180 (1970).

[7]E. J. Yarmchuck and W. I. Glaberson, J. Low Temp. Phys. 36, 381 (1979).

[8]R. J. Miller, I. H. Lynall, and J. B. Mehl, Phys. Rev. B 17, 1035 (1976).

[9]R. K. Childers and J. T. Tough, Phys. Rev. B 13, 1040 (1976).

[10]D. R. Ladner, R. K. Childers, and J. T. Tough, Phys. Rev. B 13, 2918 (1976).

[11]C. E. Oberly and J. T. Tough, J. Low Temp. Phys. 7, 223 (1972).

[12]D. F. Brewer and D. O. Edwards, Proc. R. Soc. London Ser. A 251, 247 (1959); Philos. Mag. 6, 775 (1961); 6, 1173 (1961); 7, 721 (1962); J. Low Temp. Phys. 43, 327 (1981).

[13]R. P. Slegtenhorst, G. Marees, and H. van Beelen, Physica (Utrecht) B 113, 341 (1982).

[14]J. T. Tough, Phys. Rev. Lett. 44, 540 (1980).

[15]H. Schlichting, *Boundary Layer Theory* (McGraw-Hill, New York, 1968), p. 176.

[16]Stycast 1266, from Emerson and Cuming, Inc., Northbrook, Illinois.

[17]R. M. Kimber and S. J. Rogers, Cryogenics 13, 350 (1973).

[18]S.H.E. Corporation, San Diego, California.

[19]K. P. Martin, Ph.D. thesis, Ohio State University, 1982 (unpublished).

[20]W. F. Vinen, Proc. R. Soc. London Ser. A 240, 128 (1957).

[21]D. R. Ladner (private communication).

[22]R. A. Ashton, L. B. Opatowsky, and J. T. Tough, Phys. Rev. Lett. 46, 658 (1981).

[23]L. B. Opatowsky and J. T. Tough, Phys. Rev. B 24, 5420 (1981).

[24]C. E. Chase, Phys. Rev. 127, 361 (1962).

[25]P. E. Dimotakis and J. E. Broadwell, Phys. Fluids 16, 1787 (1973).

[26]V. P. Peshkov and V. J. Tkachenko, Zh. Eksp. Teor. Fiz. 41, 1427 (1961) [Sov. Phys.—JETP 14, 1019 (1962)].

[27]D. R. Ladner and J. T. Tough, Phys. Rev. B 17, 1455 (1978); 20, 2690 (1979).

[28]J. D. Henberger and J. T. Tough, Phys. Rev. B 25, 3123 (1982).

[29]J. D. Henberger, Ph.D. thesis, Ohio State University, 1982 (unpublished).

[30]C. F. Barenghi, K. Park, and R. J. Donnelly, Phys. Lett. 84A, 435 (1981).

[31]W. F. Vinen, Proc. R. Soc. London Ser. A 243, 400 (1957).

[32]L. D. Landau and E. M. Lifshitz, *Fluid Mechanics* (Pergamon, New York, 1959).

[33]S. Uchida, Z. Angew. Math. Phys. 7, 403 (1956).